Acta Oceanol. Sin., 2024, Vol. 43, No. 1, P. 70–79
https://doi.org/10.1007/s13131-023-2202-x
http://www.aosocean.com
E-mail: ocean2@hyxb.org.cn

Observation of Arctic surface currents using data from a surface drifting buoy

Hongxia Chen[1, 2, 3], Lina Lin[1, 2, 3*], Long Fan[4], Wangxiao Yang[5, 6], Yinke Dou[5], Bingrui Li[6], Yan He[1, 2, 3], Bin Kong[1, 2, 3], Guangyu Zuo[5], Na Liu[1, 2, 3]

[1] First Institute of Oceanography, Ministry of Natural Resources, Qingdao 266061, China

[2] Laboratory for Regional Oceanography and Numerical Modeling, Pilot National Laboratory for Marine Science and Technology (Qingdao), Qingdao 266237, China

[3] Key Laboratory of Marine Science and Numerical Modeling, Ministry of Natural Resources, Qingdao 266061, China

[4] Naval Research Academy, Tianjin 300061, China

[5] College of Electrical and Power Engineering, Taiyuan University of Technology, Taiyuan 030024, China

[6] Polar Research Institute of China, Shanghai 443005, China

Received 22 September 2022; accepted 19 March 2023

Abstract

During the 10th Chinese Arctic scientific expedition carried out in the summer of 2019, the surface current in the high-latitude areas of the Arctic Ocean was observed using a self-developed surface drifting buoy, which was initially deployed in the Chukchi Sea. The buoy traversed the Chukchi Sea, Chukchi Abyssal Plain, Mendeleev Ridge, Makarov Basin, and Canada Basin over a period of 632 d. After returning to the Mendeleev Ridge, it continued to drift toward the pole. Overall, the track of the buoy reflected the characteristics of the transpolar drift and Chukchi Slope Current, as well as the inertial flow, cross-ridge surface flow, and even the surface disorganized flow for some time intervals. The results showed that: (1) the transpolar drift mainly occurs in the Chukchi Abyssal Plain, Mendeleev Ridge, and western Canada Basin to the east of the ridge where sea ice concentration is high, and the average northward flow velocity in the region between 79.41°N and 86.32°N was 5.1 cm/s; (2) the average surface velocity of the Chukchi Slope Current was 13.5 cm/s, and while this current moves westward along the continental slope, it also extends northwestward across the continental slope and flows to the deep sea; and (3) when sea ice concentration was less than 50%, the inertial flow was more significant (the maximum observed inertial flow was 26 cm/s, and the radius of the inertia circle was 3.6 km).

Key words: Chinese National Arctic Research Expedition (CHINARE), surface drifting buoy, transpolar drift, Chukchi Slope Current, inertial flow.

Citation: Chen Hongxia, Lin Lina, Fan Long, Yang Wangxiao, Dou Yinke, Li Bingrui, He Yan, Kong Bin, Zuo Guangyu, Liu Na. 2024. Observation of Arctic surface currents using data from a surface drifting buoy. Acta Oceanologica Sinica, 43(1): 70–79, doi: 10.1007/s13131-023-2202-x

1 Introduction

Oceanic currents affect various physical, chemical, biological, and geological processes in the ocean, as well as determining the climate and weather conditions, and their variation. As the most concrete manifestation of ocean currents, surface currents also have a significant impact on the climate, waterways, and fisheries. As a phenomenon formed by polar atmospheric circulation and air-ice-sea interaction in the Arctic Ocean, surface currents have special significance to the research of the navigation environment.

As a platform for observing the Lagrangian current, satellite-tracked surface drifting buoys have the advantages of being inexpensive, compact, and simple to use. They can also collect data on the ocean and weather, and are characterized by autonomous location and data transfer. Buoys represent an ideal observation platform to study the modulation of surface elements by upper-ocean processes (Centurioni, 2018), and they have been widely used to investigate upper-ocean circulation. From the perspective of ocean circulation and ocean material transport, buoys are direct and suitable tools for field observation of the surface flow.

The widely used map of the Arctic surface circulation and sea ice drift was created based on the trajectories of ice buoys and ice stations over a period of 40 years (Tomczak and Godfrey, 1994). The transpolar drift (TPD), which flows from the Siberian coast to the Fram Strait, and the clockwise Beaufort Gyre (BG) are the main characteristics of this surface circulation (Fig. S1). The European Union-sponsored DAMOCLES project, which ran from 2007 to 2009, deployed 18 ice buoys in the TPD region (Haller et al., 2014). Between August and September 2018, 27 ice buoys were positioned in the Pacific sector of the Arctic Ocean (PAO) during the CHINARE and the TICE expedition led by the Alfred Wegener Institute, Germany (Lei et al., 2021). The lack of observational data due to the limitations posed by ice coverage remains a key issue in Arctic Ocean research (Kikuchi et al., 2015).

For a short period of time in the summer, an ice-free sea area is formed in the PAO south of 80°N. Ship-based platform obser-

Foundation item: The Fundamental Research Fund Project of the First Institute of Oceanography, Ministry of Natural Resources, under contract No. GY022Y07; the National Natural Science Foundation of China under contract No. 42106232.
*Corresponding author, E-mail: linln@fio.org.cn

vations and anchored submarine observations have provided new insights into the circulation of the Chukchi Sea and the branch of inflow water deriving from the Bering Strait. For example, it was revealed that, after the branch of the Central Channel and Alaska Coastal Current separate, the two currents cross the Chukchi Sea to the north and then flow from the west to the east, finally rejoining in Barrow Canyon (Gong and Pickart, 2015). A tributary current of Pacific water that runs northward from the Central Channel bifurcates as it reaches Hanna Shoal, flows on either side of the shoal, and divides into smaller filaments toward Barrow Canyon (Pickart et al., 2016). On the Chukchi Sea shelf, the flow is mainly westward and has a velocity of around 20 cm/s (Wang et al., 2012; Gong and Pickart, 2015; He et al., 2015).

Due to the rapid melting of sea ice in summer, it is difficult to set up long-term/short-term ice stations and deploy ice buoys in the northern Chukchi Sea. Current records in the PAO north of 73.5°N and south of 85°N are very sparse and, as a result, current dynamics in the sea north of the Chukchi slope are not sufficiently clear. Observational data based on drifting buoys are very scarce, especially in ice-free sea during the summer (Centurioni et al., 2017).

In August 2019, during the CHINARE, surface current observations were conducted using drifting buoys and one of them (with iridium No. 3002340100701500) was released in the northern Chukchi Sea. While in operation between September 2, 2019, and June 9, 2021, this buoy monitored the Chukchi Sea, Chukchi Abyssal Plain (CAP), Makarov Basin, Mendeleev Ridge, and Canada Basin. The data obtained can greatly contribute to the understanding of the dynamics of surface currents flowing from the northern Chukchi Sea to the high-latitude areas of the Arctic Ocean. The present study examined surface currents in various locations in the Arctic Ocean based on these buoy data, taking into consideration criteria such as buoy trajectory characteristics and sea surface conditions.

2 Data and method

The drifting buoy used in this study was provided by Taiyuan University of Technology, China, and its main technical features are: (1) GPS positioning with a maximum inaccuracy of 2.5 m; (2) iridium transmission with a 4-hour transmission interval and 340 bytes per transfer; (3) continuous working period of more than 2 years and sampling frequency of 1 h; and (4) data transmission via single repeat sending.

The total drift distance of the buoy throughout the 632-day observation period exceeded 6 646 km, excluding two periods in which recordings were missing (from 0:00 on January 1 to 17:00 on January 6, 2021, and from 4:00 on November 12 to 13:00 on November 20, 2020). The original records have both duplicated and missing data, which were checked and deleted before the calculation of flow velocity and flow direction, and only one valid record per hour was retained. In addition, to ensure the reliability of the original data, no internal interpolation was performed when valid records were missing. Ultimately, 14 754 usable records were retrieved, accounting for 97.3% of the total.

Flow velocity was calculated when the time interval was less than 6 h, and the velocity value was assigned to the time. The accuracy of velocity calculations was ±2.1 cm/s for 1-hour intervals and ±2.0 cm/s for 6-hour intervals (Chen et al., 2021). Considering that the period of the inertial current is about 12 h in this area, and the tidal current in the Chukchi Sea is mainly semidiurnal (Wang et al., 2011), a 12-hour sliding average residual flow was calculated to filter out these periodic currents.

To analyze the trajectory and velocity characteristics of the buoy in detail, velocity and flow direction were also determined in different periods based on sea area, trajectory, and sea surface conditions (Table 1).

Additionally, the present study used the following datasets: the ERA5 sea surface wind field data from the European Centre for Medium-Range Weather Forecasts, the sea ice data from NASA and the National Snow and Ice Data Center, the daily average of sea ice density data obtained from the microwave remote sensing AMSR2 (University of Bremen, Germany), and seven datasets obtained from ice drifting buoys deployed in 2018 in the Makarov Basin (Alfred Wegener Institute, Germany).

3 Characteristics of buoy trajectory and velocity

3.1 *Analysis of buoy trajectory and velocity over the whole observation period*

Figure 1 shows that the drifting path of the buoy was relatively complex throughout the entire period. The track reflected not only the general characteristics of the northward TPD, but also those of the Chukchi Slope Current (CSC), inertial flow, cross-ridge surface flow and, occasionally, even the surface disorganized flow. The buoy began to drift from the northern part of the Chukchi Sea and traveled across this sea, the CAP, Mendeleev Ridge, Makarov Basin, and Canada Basin. After returning to the Mendeleev Ridge, it continued to move toward the North Pole along this ridge.

Statistics showed that the maximum, minimum, and average values of the 1-hour velocity were 61.07 cm/s, 0.04 cm/s, and 12.71 cm/s, respectively. The maximum, minimum, and average velocity values of the 12-hour sliding average residual flow were 50.38 cm/s, 0.07 cm/s, and 11.03 cm/s, respectively. Specifically, Table 2, which reports the velocity in each section, shows that the highest values were in the range of 5–10 cm/s, accounting for 28.2% of the total record number, and that the ratios were 18.8%

Table 1. Division of sections, median values and maximum values of drift residual speed for different sections of the drifting buoy

Section No.	Duration	Starting position	End position	Drift residual speed/(cm · s^{-1})		Figure No.	Main characteristic
				Median value	Maximum value		
001	Sept. 2–Sept. 30, 2019	74.69°N, 168.99°W	75.87°N, 174.97°W	12.71	32.78	5, 6	inertial flow
002	Oct. 1, 2019–Feb. 19, 2020	75.87°N, 174.95°W	76.33°N, 175.89°W	12.62	50.38	6	disorganized surface flow
003	Feb. 19, 2020–Jun. 18, 2020	76.33°N, 175.89°W	79.86°N, 170.20°W	8.79	28.45	3	transpolar drift
004	Jun. 18–Sept. 24, 2020	79.86°N, 170.20°W	79.41°N, 179.89°E	12.02	39.09	10	surface cross-ridge flow
005	Sept. 24–Nov. 11, 2020	79.41°N, 179.89°E	81.70°N, 178.31°E	12.81	31.92	3	transpolar drift
006	Nov. 20–Dec. 31, 2020	81.41°N, 174.76°W	82.15°N, 173.42°W	10.49	35.83	4, 6	transpolar drift; inertial flow
007	Jan. 6–Mar. 10, 2021	82.06°N, 171.21°W	82.75°N, 177.47°W	10.44	46.83	7	disorganized surface flow
008	Mar. 10–Jun. 9, 2021	82.75°N, 177.47°W	86.32°N, 150.85°W	8.88	30.63	4	transpolar drift

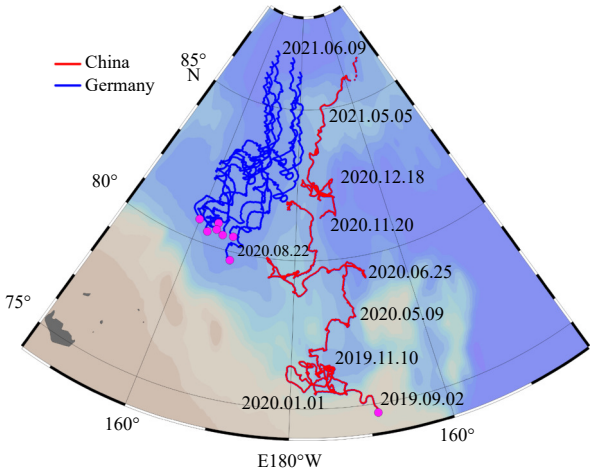

Fig. 1. Drift trajectories of buoys. The red line is the trajectories of drifting buoys deployed by CHINARE, and the blue lines are the trajectories of 7 ice buoys deployed by the Alfred Wegener Institute, Germany. The rose dots represent the starting points of the buoys' trajectories.

and 5.0% for velocities greater than 20 cm/s and 30 cm/s, respectively. In comparison, the number of records with residual velocities within the range of 5–10 cm/s increased, accounting for 32.0% of the total record number, while the ratio decreased significantly to only 12.0% for residual velocities greater than 20 cm/s.

All flow directions appeared in both the 1-hour flow and residual flow records (Fig. 2). Statistical analysis of the former indicated that northeast, north, and northwest were the dominant flow directions, with a total ratio of 49.3%, while south and southwest were detected at lower ratios of 9.2% and 8.1%, respectively. Similarly, in the analysis of the latter, northeast, north, and northwest continued to be the dominating flow directions, with a total ratio of 50.0%, and south and southwest still had relatively low ratios of 8.6% and 8.1%, respectively.

Further comparisons revealed that both the maximum and average velocities decreased significantly after the 12-hour sliding average residual flow, while flow direction did not change considerably. In fact, the significant reduction of the record ratio of velocity by more than 20 cm/s suggests that the relatively rapid drift of the buoy was likely to be a temporary process caused by a transient weather event. When buoys are located in the open ocean, polynyas, or ice water channels, short and severe weather events will cause them to drift rapidly. The small statistical difference in flow direction detected in this study indicated that this parameter is less significantly affected by short-period currents, such as inertial and tidal currents.

3.2 *Transpolar drift*

The TPD and BG are two major near-surface current systems in the Arctic Ocean. The former originates off the Siberian coast, travels through the central Arctic Ocean, and finally enters the Fram Strait. It transports about 3 000 km^3 of sea ice from the Arctic to the North Atlantic Ocean each year, and also brings trace elements from Siberian rivers and continental shelves to the central Arctic Ocean, which play an important role in material exchange and thermal equilibrium (Haller et al., 2014; Tian et al., 2021). With global warming, the Arctic sea ice is rapidly receding and the location and intensity of the TPD are undergoing significant changes (Tian et al., 2021).

The Arctic Central Passage (ACP), which spans from the Bering Strait to the Fram Strait, has a good consistency with the TPD. Since the velocity of the transpolar current of last year directly affects the minimum extent of sea ice in September of the next year, and the strong transpolar current makes the residence time of sea ice in the Arctic Ocean shorter (Haller et al., 2014), the

Table 2. Percentage statistics of 1-hour velocity and residual velocity in cm/s with an interval of 5 cm/s

Velocity type	Percentage								
	(0 cm/s, 5 cm/s]	(5 cm/s, 10 cm/s]	(10 cm/s, 15 cm/s]	(15 cm/s, 20 cm/s]	(20 cm/s, 25 cm/s]	(25 cm/s, 30 cm/s]	(30 cm/s, 35 cm/s]	(35 cm/s, 40 cm/s]	(>40 cm/s)
1-hour velocity	19.0%	28.2%	21.0%	13.0%	8.8%	5.0%	2.6%	1.1%	1.3%
Residual velocity	21.2%	32.0%	22.6%	12.1%	6.6%	3.2%	1.1%	0.7%	0.4%

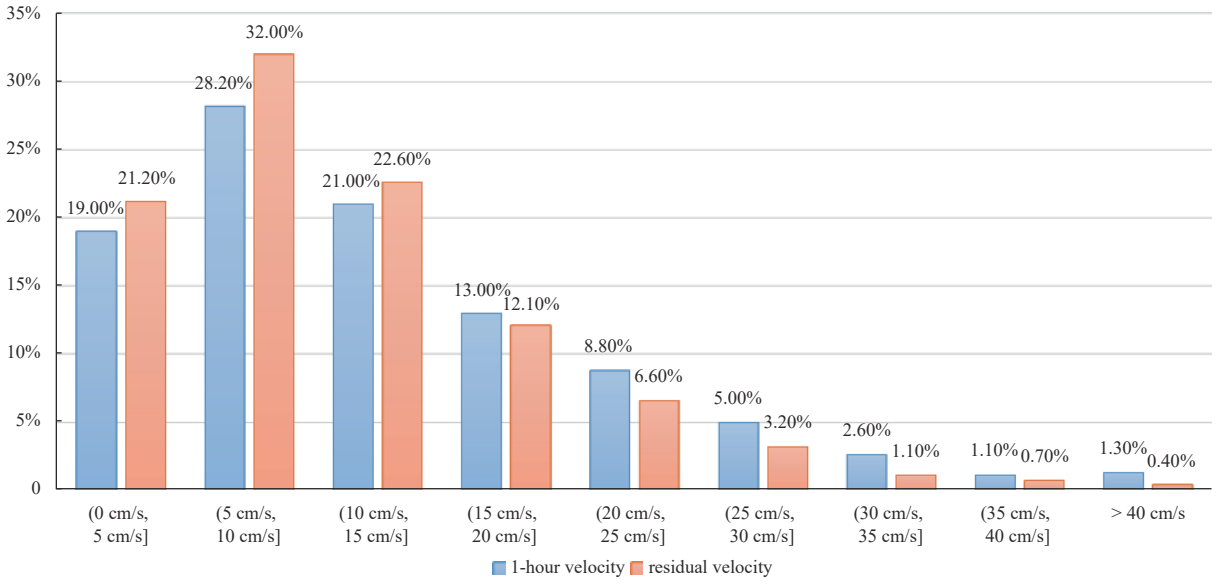

Fig. 2. Percentage statistics of 1-hour velocity and residual velocity in cm/s with an interval of 5 cm/s.

transpolar current plays a direct role in the opening and utilization of the ACP.

Previous studies have reported that the average velocity of the TPD north of 85°N was 7.5 cm/s and that between 85°N and the Fram Strait was 13.0 cm/s (Haller et al., 2014). However, the TPD from the Siberian Sea to 85°N, which is the sea area monitored in the present study, has been rarely investigated.

Figure 1 and Table 1 show that, during the whole study period, four sections of buoy trajectories—namely, the third, fifth, sixth, and eighth—exhibited significant TPD characteristics.

The third section was situated in the middle of the freeze-up period (Fig. 3a and Fig. S2). At this time, the buoy was blocked in the dense ice of the CAP, and wind conditions on the sea surface were changeable. The buoy mainly drifted northward by 3.53° of latitude through the passage for a total drift distance of 1 004.1 km. The average and maximum velocities of the residual flow were 8.8 cm/s and 28.5 cm/s, respectively. Velocity values were primarily concentrated in the range of 0–10 cm/s, and the ratio of values >20 cm/s was only 1.6%. The average northward velocity in the third section was 3.5 cm/s (Table 3).

The fifth section was located in the freeze-up period, and the ice edge line gradually moved southward from 78°N to 76°N (Fig. 3b and Fig. S2). The sea was mainly affected first by west-southwesterly and then by southerly winds. In this section, the buoy was trapped in the dense sea ice at the Mendeleev Ridge, and moved northward by 2.48° of latitude for a total drift distance of 590.2 km. The maximum and average velocities of the residual flow were 31.9 cm/s and 12.8 cm/s, respectively. The values were mostly concentrated between 5 cm/s and 15 cm/s and the ratio of velocities >20 cm/s was 20.4%. North, northeast, and northwest were the main flow directions and the average northward velocity was 6.6 cm/s (Table 3).

The sixth section corresponded to the beginning of the ice period, and the buoy was located in a dense sea ice area in the western Canada Basin, east of the Mendeleev Ridge (Fig. 4a). The sea surface was mainly exposed to southerly winds with a relatively high speed. The buoy drifted 388.1 km northward over a period of 41 d, covering 1.22° of latitude. The maximum and average velocities of the residual flow were 35.8 cm/s and 10.5 cm/s, respectively. The values were mainly concentrated between 0 cm/s and 15 cm/s, and the ratio of velocities >20 cm/s was 10.3%. In the five days from November 29 to December 3, the buoy mainly drifted northward at an average speed of 22.1 cm/s. Between 81.4°N and 82.7°N in the western Canada Basin, the average northward speed was minimal and flow direction was variable, therefore this region was not considered as a part of the TPD. The average northward velocity in the third section was 3.8 cm/s (Table 3).

The eighth section was located in the middle to late ice period, and the buoy was positioned in a dense sea ice area at Mendeleev Ridge (Fig. 4b). The sea surface at this time was exposed to a steady southerly breeze with a speed of around 6 m/s. The buoy moved 752.6 km northward covering 3.47° of latitude. The maximum and average velocities of the residual flow were 30.6 cm/s and 8.9 cm/s, respectively. The values were mainly concentrated between 0 and 15 cm/s, and the ratio of velocities >20 cm/s was 17.2%. The buoy consistently drifted northwestward at an average speed of 4.9 cm/s (Table 3), showing that the TPD is predominant in the Mendeleev Ridge area north of 82.7°N.

From the perspective of drift direction stability, the second half of the third and eighth sections showed the most notable TPD characteristics. In terms of northward drift speed, the magnitude was basically consistent with in the previous studies. After reaching 85°N on May 3, 2021, the drift velocity of the buoy was 7.3 cm/s in a northeast direction. This is consistent with the average transpolar flow north of 85°N (Haller et al., 2014). In this paper, the average northward speed was 5.1 cm/s between 79.41°N and 86.32°N, which is generally consistent with the TPD velocity (~4.8 cm/s) obtained from seven ice buoys located between 80°N and 85°N, which were deployed on the Makarov Basin by the Alfred Wegener Institute in 2018 (Table 4).

By combining the trajectories and sea areas of these seven ice buoys, it was revealed that the buoy used in this study was also

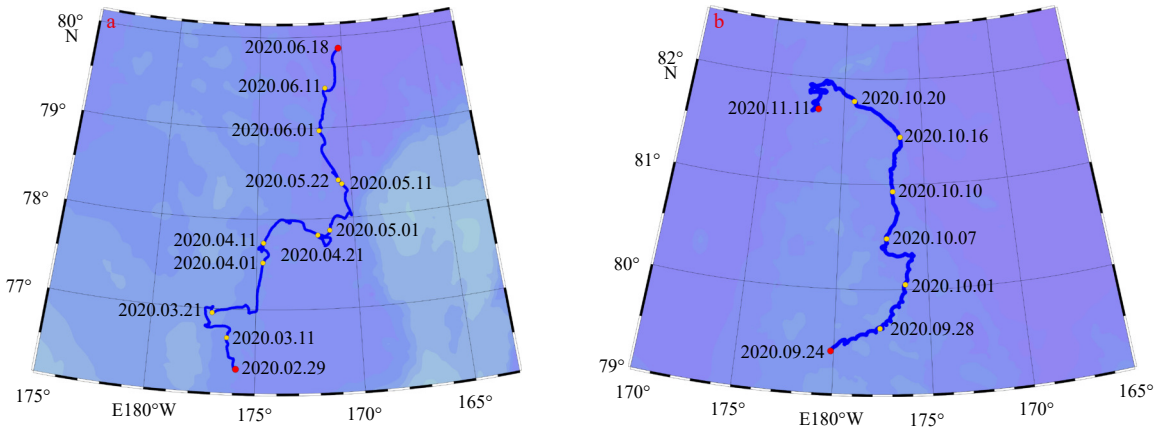

Fig. 3. Drift buoy trajectory in the third section (a) and the fifth section (b). The red dots represent the starting and ending points of the buoys' trajectories, respectively.

Table 3. Average northward velocity of transpolar drift in each period

Section No.	Month range	Zonal range	Average northward velocity/(cm·s^{-1})
003	Feb.–Jun.	76.33°–79.86°N	3.5
005	Sept.–Nov.	79.41°–81.70°N	6.6
006	Nov.–Dec.	81.41°–82.15°N	3.8
008	Mar.–Jun.	82.75°–86.32°N	4.9

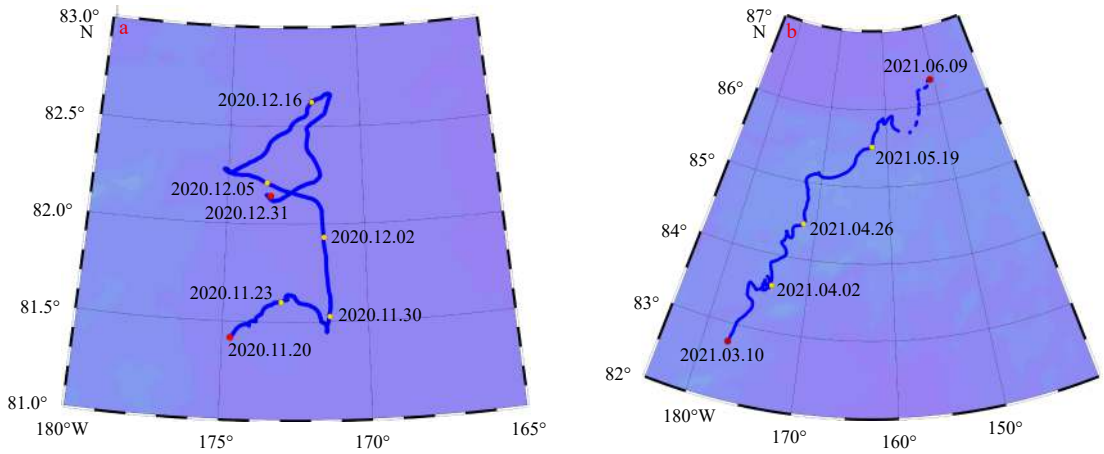

Fig. 4. Drift buoy trajectory in the sixth section (a) and the eighth section (b). The red dots represent the starting and ending points of the buoys' trajectories, respectively.

located in the transpolar region and it could similarly reflect the movements of the ice surface during the ice period.

Considering that the four sections examined were all covered by sea ice, the buoy should be trapped in the ice as well and drift along with it. Substantial surface winds were accompanied by strong sea surface stresses and high TPD speeds. The differences in drifting characteristics in the four sections not only reflected the variation of surface currents in different sea areas, but also confirmed the large differences in the features of the surface transpolar current at both the monthly and seasonal time scales.

3.3 *CSC*

The CSC is a fast channel that transports Pacific Ocean water to the Arctic Ocean at a high flux through Barrow Canyon. It is mainly composed of Pacific winter water, Alaska coastal water, Bering Sea summer water, and Atlantic water (Corlett and Pickart, 2017). Pacific waters have a significant impact on sea ice, water masses, and circulation in the Arctic Ocean (Shi et al., 2004). They play an important role in melting and delaying the formation of continental shelf ice (Weingartner et al., 2005) and basin ice (Steele et al., 2010; Woodgate et al., 2012; Brugler et al., 2014); in addition, they directly affect the Arctic ecosystem (Corlett and Pickart, 2017) and greatly influence the structure of the upper ocean (Killworth and Smith, 1984), with effects extending from the Arctic to the northern Atlantic Oceans (Jones et al., 2003).

The study of circulation on the continental shelf of the Chukchi Sea is at its initial stage. In 2017, Corlett and Pickart (2017) identified the CSC for the first time based on dynamic calculation results. The study also found that this current is surface-intensified (<15 cm/ s), has a width of about 50 km, and has an average westward flux of (0.50 ± 0.07) × 10^6 m^3/s. In 2019, Li et al. (2019) further confirmed the existence of the CSC based on a year-long mooring array across the shelfbreak/upper-slope of the Chukchi Sea and estimated that the current transports (0.57 ± 0.04) × 10^6 m^3/s of Pacific water. This flow is present throughout the year; in the summer and fall, it is surface-intensified while, in the winter and spring, it is middepth-intensified, flows shoreward, and finally diminishes.

Table 4. Average northward velocity (80°–85°N) in each latitude calculated from 7 ice buoys records deployed during TICE expedition

Buoy No.	Start latitude	Average northward velocity/(cm·s^{-1})
2018S75	80.50°N	4.4
2018S76	80.70°N	4.3
2018T35	80.50°N	4.3
2018T46	80.44°N	4.7
2018T52	80.78°N	5.0
2018T54	79.66°N	5.0
2018T55	80.75°N	5.8

Sectional hydrological data and mooring array data present inherent advantages for flow calculation, identification of water masses, and characterization of flow microstructure, but they have also inherent deficiencies for flow path identification that are associated with their observation range. In contrast, drifting buoy data are particularly suited for flow path identification. In the present study, the first section of the trajectory was September 2–30, 2019. According to data released by the NSIDC in December 2019, the extent of Arctic sea ice in the summer of 2019 was the second lowest detected over the entire 41-year satellite recording period. The buoy in this section was located in the open water and its drift reflected the surface currents of the ice-free Chukchi Sea.

The buoy drifted 387.1 km over a period of nearly one month in this section (Fig. 5). The overall direction was northwestward and velocity values were mainly concentrated between 5 cm/s and 20 cm/s. The maximum and average residual velocities were 32.8 cm/s and 12.7 cm/s, respectively. Before September 16, the flow was mainly northward between 74.7°N and 75.3°N near 169°W and a subsequent Ω-shaped flow-sleeve drift. The buoy drifted westward roughly along the continental slope between 170.70°W and 174.36°W from September 16 to 22. After September 22, in the vicinity of 174.36°W, the buoy departed from the continental slope and drifted into the CAP.

The average drifting speed of the buoy (13.5 cm/s) matched almost perfectly the velocity obtained from dynamic calculations (<15 cm/s). This section of trajectory may represent the route of the CSC west of 169°W when the sea is open, and may extend it northwestward by nearly 400 km. This trajectory reflects the complex characteristics of the CSC, which flows not only westward along the slope, but also across the slope toward the deep sea.

This shows that the Pacific water from Barrow Canyon continues to expand westward with the CSC. It extends to the northwest and affects the CAP simultaneously, and continues to extend northwestward within the CAP. The trajectory of the buoy indicates where the Pacific water enters the inner part of the Arctic Ocean from the continental shelf and the route it crosses over the

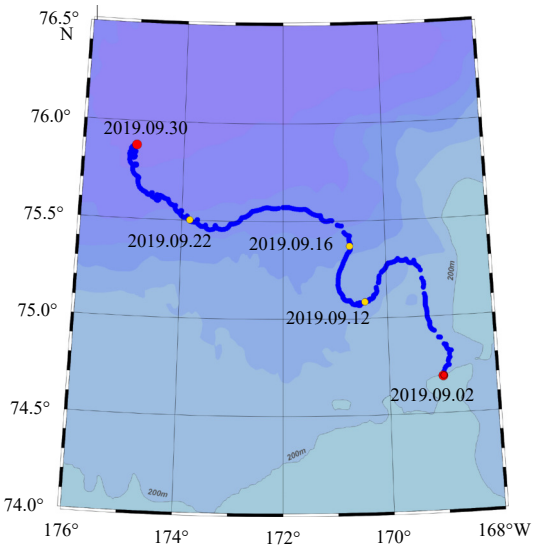

Fig. 5. Drift buoy trajectory in the first section. The red dots represent the starting and ending points of the buoy's trajectory, respectively.

continental slope of the Chukchi Sea. The path is roughly parallel to the ice edge line west of the Chukchi Plateau, which supports the direct contribution of the CSC to sea ice melting in this area. These observations further demonstrate the significant contribution of the warmer and fresher Pacific water to the offshore freshwater accumulation in the Beaufort Gyre during late spring and summer (Jones et al., 2003).

3.4 *Inertial flow*

The inertial flow is an unforced free flow that occurs in the ocean. Once an external disturbance drives the movement of a water mass, this will deflect under the action of the Coriolis force, forming a periodic rotating flow. As one of the most common flows in the ocean, the inertial flow generally has the largest amplitude in the deep ocean with non-strong currents. Therefore, the inertial flow is essential for the analysis of actual data obtained from currents (Liu, 2014). The trajectory of the inertial current is a circle, rotating clockwise in the northern hemisphere and anticlockwise in the southern hemisphere. Its radius is inversely proportional to latitude (i.e., the higher the latitude, the smaller the radius) and its period decreases with the increase of latitude. The inertial flow is an important dynamic process in the ocean and an obvious manifestation of the response of the internal ocean to the external wind field. It is mostly induced by the rapid variation of sea surface winds, which often intensifies it (Webster, 1968).

Early observations of the inertial flow were mainly carried out using an anchored current meter. In more recent times, with the development of satellite positioning technology, the drift trajectory of sea buoys was used instead to analyze this phenomenon (Poulain et al., 1992; Thomson et al., 1998; Zhao et al., 2011). The positioning time interval of the commonly surface drifting buoy is generally 6 h, and this buoy is rarely deployed in the Arctic region. To prolong the observation period and reduce communication costs, most of the other buoy platforms have a positioning time interval of about 3 h, which produces data that are unsuitable for inertial flow analysis. In the present study, the time interval between buoy recordings was only 1 h, which allowed to analyze the surface inertial current at different locations.

Previous studies have shown that the drift trajectory of floating ice in the Arctic Ocean (87°N, 175°W) in August 2010 had a circular inertial motion superimposed on the linear drift, an inertial period of about 12 h, and a maximum amplitude of the inertial flow of up to 20 cm/s (Shu et al., 2012). In the Fram Strait (~79°N), the latter decreased from about 24 cm/s at the surface to about 8 cm/s at the bottom (Liu, 2014). North of 75°N, the inertial period was also about 12 h long. In the present study, the inertial flow was analyzed based on the original data before the 12-hour sliding average residual flow. Considering the large trajectory spanning over a long period of time and wide range, only some portions exhibiting a significant inertial flow were used for the analysis of velocity.

Clockwise spiral trajectories were particularly common in September 2019, when the buoy records were continuous and the residual flow was relatively stable. The buoy trajectory from September 21 to 30, 2019 is shown in Fig. 6a. As the tidal ellipse in this sea area is counterclockwise (Wang et al., 2011) and the tidal current in the deep water of Arctic Ocean is relatively small (Shu et al., 2012), it was inferred that the clockwise spiral trajectory with a ~12-hour period was caused by the inertial flow. Firstly, the background flow is obtained by filtering method, and then the background flow is subtracted from the measured data to get the inertial flow. Two specific days with significant spiral trajectories were selected: on September 22, 2019, the residual flow was 12.2 cm/s, the inertial flow was 17.5 cm/s, and the inertia circle radius was 2.4 km; and on September 29, the same parameters were 11.1 cm/s, 25.5 cm/s, and 3.6 km, respectively.

The clockwise spiral trajectory was also common in October and November 2019, and it was difficult to determine when the sea ice concentration was higher than 50% in December (Fig. S2). Two typical days with a relatively stable residual flow in October

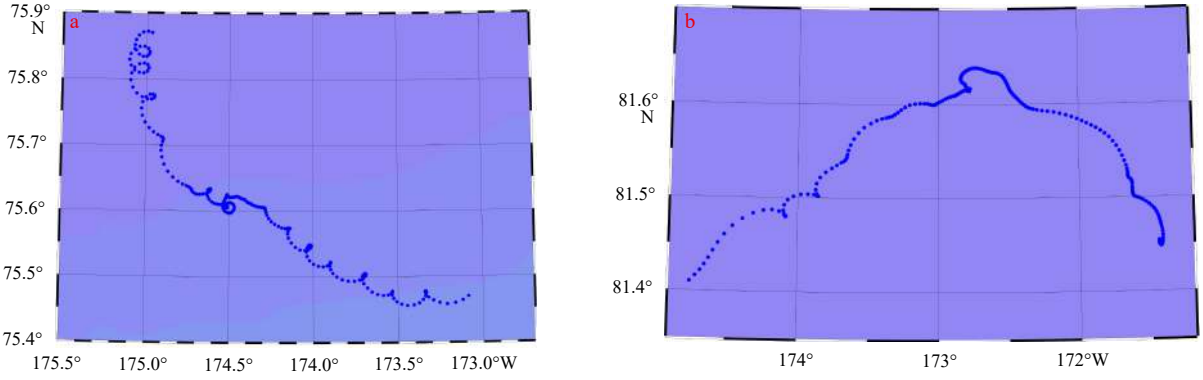

Fig. 6. Drift buoy trajectory in two ten-day periods: 2019.09.21–2019.09.30 (a) and 2020.11.20–2020.11.29 (b).

were selected for residual and inertial flow decomposition: on October 13, the residual flow was 10.1 cm/s, the inertial flow was 11.3 cm/s, and the radius of inertia circle was 1.6 km; and on October 29, the same parameters were 31.5 cm/s, 19.2 cm/s, and 2.6 km, respectively.

After July 29, 2020, the clockwise spiral or wave-shaped trajectory caused by the inertial flow reappeared. July 30, August 30, and September 29 were selected as typical days for decomposition analysis. On these days, the residual flow, inertial flow, and radius values were 16.3 cm/s,15.1 cm/s, and 2.2 km (July 30); 15.0 cm/s, 12.9 cm/s, 1.8 km (August 30); and 13.7 cm/s, 14.7 cm/s, and 2.0 km (September 29), respectively. Until the end of November, the influence of the inertial flow on the trajectory of the buoy was still significant (Fig. 6b). On November 22, the residual flow was 13.3 cm/s, the inertial flow was 7.4 cm/s, and the inertial circle radius was 1.0 km.

Combined with the distribution of sea ice, when the concentration of sea ice was less than 50%, the clockwise spiral or undulation trajectory caused by the inertial flow was more significant. The observed inertial flow can reach a maximum of 26 cm/s, and the radius was 3.6 km. The magnitude of the inertial flow has nothing to do with the residual current, but with the sea surface openness.

In terms of the magnitude of the inertial flow, the values obtained in this study were consistent with the maximum values reported at higher latitudes (87°N, 175°W) in August 2010, and were slightly lower than those measured in the Fram Strait. This also confirms that surface drift buoys are adequate tools for inertial flow observation.

3.5 *Disorganized surface flow*

In the second and seventh sections, i.e., from October 1, 2019, to February 29, 2020, and from January 6 to March 9, 2021, respectively, the buoy trajectories were particularly chaotic (Fig. 7). The flow departed in all directions but did not exhibit either the vortex or turbulence characteristics. Such disorder was most significant in the second section, and the reentrant flow from the southeast to the northwest was dominant in the seventh section.

Based on sea ice concentration data, in October 2019 the buoy was still in the open sea in the second section. In November 2019, the monthly average sea ice concentration in the area where the buoy located was 40%–60%. After December 1, 2019, the ice edge line in the Chukchi Sea rapidly expanded to the south, and the buoy was located to the north of the monthly average ice edge line. February 2020 corresponded to the local ice period and, at this time, the seventh section was completely covered with dense sea ice.

The term “disorganized” here refers to a flow in which the magnitude and direction of the water mass movement change complexly without significant regularity over a long period of time, but remain regular in the short term. The scale of the disorganized flow is significantly larger than that of the turbulent one, in which the magnitude and direction of the water movement fluctuate chaotically, and the two flows are not the same phenomenon. Although the disorganized flow that repeatedly turns back in a certain direction sometimes occurs, at this time it is not a reciprocating flow with the opposite (or almost opposite) direction of ebb and flow due to the influence of the terrain.

The disorganized flow can enhance the diffusion of substances, the dispersion and transfer of momentum and heat, and promote the local horizontal mixing of water masses, which in turn affects their vertical mixing and cline distribution. At the same time, this type of flow has a great impact on data collection, affecting not only safety during operations at sea, but also the quality of the collected data (Yi et al., 2019). The complexity of the disorganized flow is rarely studied, not only in the Arctic Ocean, but also in other seas.

Statistical analysis revealed that the predominant flow direction in the second section was southeastward (16.4%), while the southwestward one was the least detected (9.1%), and the other directions were relatively balanced (10.6%–14.7%). In the seventh section, the southward and southwestward flow directions (6.5% and 6.3%, respectively) were less detected than the northward and northwestward ones (17.9% and 18.2%, respectively), and the other directions were relatively balanced (10.4%–14.3%). Figure 8 indicates that the flow was relatively low with average values of 12.6 cm/s and 10.4 cm/s respectively and the velocity records were mainly concentrated between 5 cm/s and 20 cm/s in the second and seventh sections, which did not decrease significantly due to the change in flow direction and were still comparable to those of the third and sixth sections. For these, the velocity records were mainly concentrated between 5 cm/s and 20 cm/s, with average values of 12.6 cm/s and 10.4 cm/s, respectively, which did not decrease significantly due to the change of flow direction.

During the 142-day period covered by the second section, the absolute distance of the buoy drift was only 47.6 km and the ratio to the total drift distance (1 853.9 km) was only 2.5%. During the 65 d covered by the seventh section, the same parameters measured 104.4 km and 22.1% (ratio to 472.1 km), respectively. The

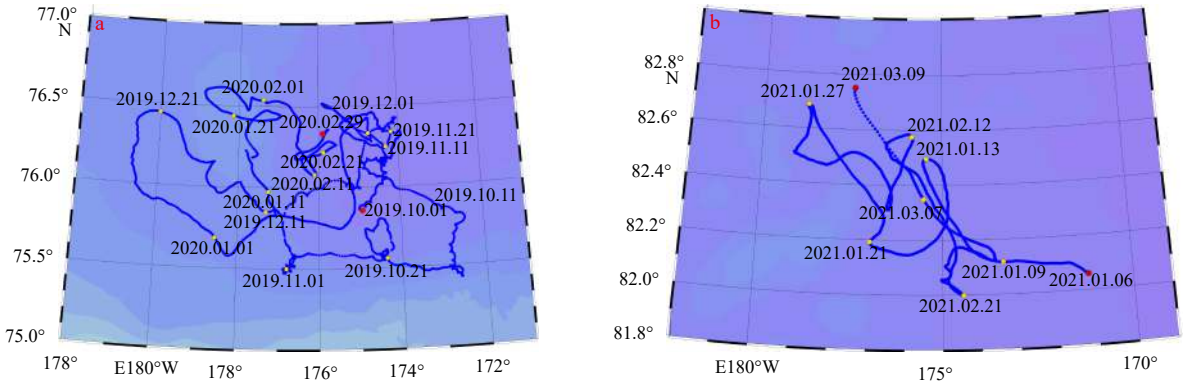

Fig. 7. Drift buoy trajectory in the second section (a) and the seventh section (b). The red dots represent the starting and ending points of the buoys' trajectories, respectively.

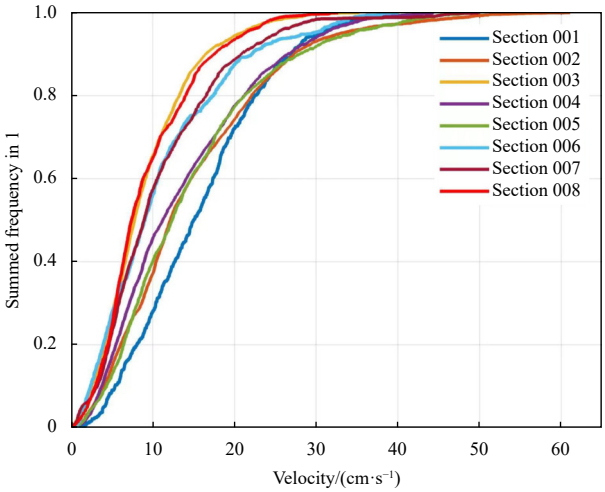

Fig. 8. Histograms of drift velocity in different sections.

trajectories of these two sections respectively reflected the changeable drift of the buoy in the open waters of the CAP before and after the early ice period, and in the western region of the Canada Basin on the eastern side of the Mendeleev Ridge after the buoy froze unto the ice surface.

By comparing the drift and wind at 75.5°N, 174.75°W between October 2019 and February 2020 (Fig. 9), it is clear that there was a very good synchronization correlation between them, even though the wind speed and direction were variable during this period. On the one hand, it indicates that the geostrophic current is weak and wind plays a decisive role in sea currents. On the other hand, it indicates the immediacy of response of surface flow field to wind.

The Ekman surface flow (Sverdrup et al., 1942) was calculated based on the local average wind speed of 6.1 m/s in the sea area where the buoy was located (~75.5°N) and it was about 8.1 cm/s, while the Ekman layer depth was 25.2 m. Considering that this flow speed corresponded to 55% of the drift speed of the buoy, and that the average drift direction shifted 17.6° to the right relative to wind direction, it was gathered that the empirical formula used to calculate the Ekman surface flow has certain limitations. Due to the influence of the sea surface ice and change of wind direction, the driving of wind did not reach a geostrophic equilibrium, and the offset angle was less than 20°. The drifting of the buoy reflects the speed of the sea surface when this is a mix of ice and water, and the driving effect of the wind in these conditions is greater than that in open sea conditions, so the speed was greater than that at this time.

The seventh section presented a similar situation and will not be discussed here. Overall, these two sections showed a complex surface flow, and the surface wind during their periods had a dominant effect on the surface current (ice drift).

3.6 *Surface cross-ridge flow*

The period from June 18 to September 24, 2020, corresponded to the end of the ice and ice-melting periods (Fig. 10 and Fig. S2). The positioning and sea ice density data of the buoy at this time revealed that the buoy was located north of the ice edge line and the ice concentration in the area was greater than 75% before August 16. From August 16 to September 7, the buoy was located in an area with ice concentrations between 25% and 75%. After September 7, it moved near the ice edge line and returned to the open sea. The sea was first dominated by westerly winds, then by northerly winds (Fig. 11).

This section showed the most significant westward and northwestward drift compared to all the other sections (Fig. 11). The drifting range of the buoy was mainly between 79°N and 80°N. The buoy was first located in the Canada Basin in the east, then it reached the Makarov Basin in the west, and finally crossed the Mendeleev Ridge from east to west. Overall, it moved westward and northwestward across the ridge.

Over a period of 98 d, the total drift distance of the buoy was as high as 1 152.4 km and the east-to-west span reached 360.2 km. The maximum value of the residual flow was 39.1 cm/s and the ratio of records with velocities >20 cm/s was 14.1%. The ratio of records with velocity values >30 cm/s was 3.7%, all of which showed either an eastward or westward direction. The velocity records were mainly concentrated between 5 cm/s and 15 cm/s, with an average value of 12.0 cm/s; the main direction was south-

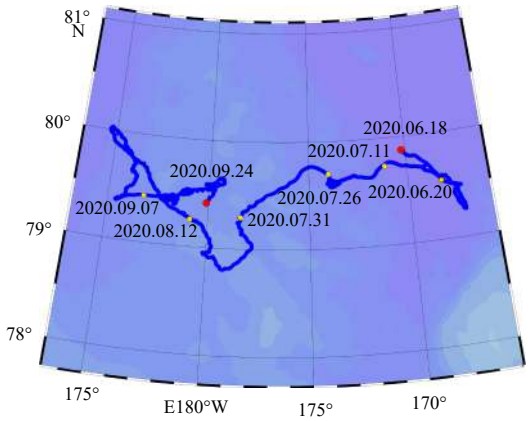

Fig. 10. Partial track of the drifting buoy (June 18, 2020–September 24, 2020). The red dots represent the starting and ending points of the buoy's trajectory, respectively.

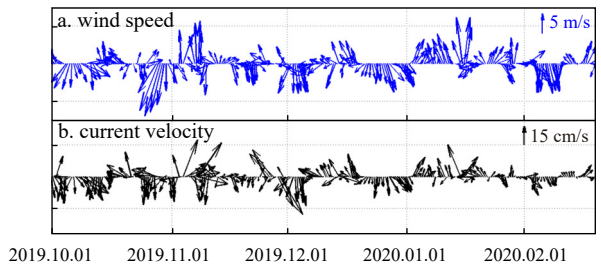

Fig. 9. Diagram of ER5 wind speed and direction at point (75.50°N, 174.74°W) (up), velocity and flow direction in the second period (down).

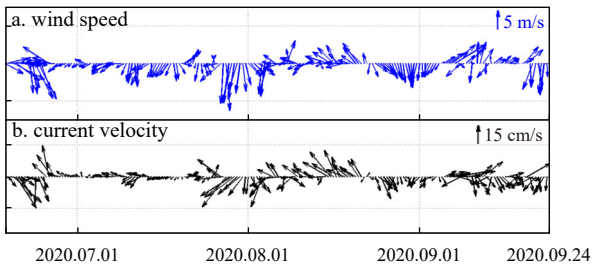

Fig. 11. Diagram of ER5 wind speed and direction at point (79.5°N,178°W) (up), velocity and flow direction in the fourth section (down).

westward, westward, and northwestward (49%).

Between June 22 and July 31, 2020, the buoy drifted westward from the Canada Basin near Mendeleev Ridge. This relatively stable westward flow, with an average velocity of 6.5 cm/s, was the most prominent feature of this period, which was also characterized by southwesterly winds with an average speed of 5.1 m/s. The velocity of the Ekman surface flow was 6.6 cm/s, which is consistent with the above-mentioned average westward velocity. Between August 5 and 23, 2020, the buoy drifted northwestward from the Mendeleev Ridge to the Makarov Basin. This northwestward flow, with an average velocity of 15.0 cm/s was the most important feature of this period, during which the wind was mainly westerly, with an average speed of 4.9 m/s. The velocity of the Ekman surface flow was calculated as 6.3 cm/s, which corresponded to only 42% of the average drift speed.

The combination of the sea ice distributions of the two abovementioned periods revealed that, when the sea ice concentration was ⩾75%, the drift speed was consistent with the values calculated using the empirical formula; in contrast, when it was between 25% and 75%, the drift speed was considerably greater than the calculated one. This indicated that, when the ice concentration in this area is high, the Ekman surface flow is the main component of buoy drifting; whereas, when it is low, the surface current mainly consists of flows other than the Ekman surface current.

Northwesterly winds prevailed from August 16 to 22, while southerly winds prevailed from August 30 to September 4, 2020. By including the drift speeds of these two periods in the comparison, it was observed that, during the former period, the Ekman surface flow (7.4 cm/s) was only 43% of the drift speed of the buoy (17.3 cm/s), and the drift direction was 15.6° to the left of the wind. During the latter, the Ekman surface flow (5.7 cm/s) reached 69% of the drift velocity of the buoy (8.2 cm/s), and the drift direction was 12.9° to the right of the wind. This indicated that the surface currents, except for the Ekman drift, move westsouthwestward when the sea surface is relatively open.

By combining the location of the sea ice edge over the years and the direct contribution of the inflowing warm water to ice melting, it was inferred that this sea area is affected by the Pacific warm water, and there is a west-southwestward surface flow in the southern portion of the Mendeleev Ridge. Under the combined action of surface currents and surface winds, the Pacific inflow water is transported from the Canada Basin to the Makarov Basin. Given that the latter is the main channel of the TPD, the surface seawater will flow from the BG area to the TPD area.

The surface of the Mendeleev Ridge is primarily characterized by the transpolar current and Canadian Basin Beaufort vortex along the direction of the ridge on its western side, while the lower Atlantic water is transported along the isobath and clockwise from the west to the east (Woodgate et al., 2007). The cross-ridge surface flow in this area has not been mentioned in existing studies. Combined with the analysis of the sources of rare earth elements in the Mendeleev Ridge (Zhao et al., 2020), the trajectory of this flow not only directly confirms the source of material input, but also represents a meridional transport of surface seawater to the ridge.

4 Conclusions

Since the buoy began working in the northern Chukchi Sea, the buoy passed through the Chukchi Sea, the CAP, Mendeleev Ridge, Makarov Basin, and Canada Basin. After returning to the Mendeleev Ridge, the buoy continued to advance toward the North Pole along the ridge over a period of 632 d. The drift distance of the buoy was more than 6 646 km, and the drift route was relatively complex. Overall, the trajectory of the buoy reflected the northward flow characteristics of the TPD and those of the CSC, as well as the inertial flow, surface cross-ridge flow, and even the disorganized surface flow in a local period.

Throughout the whole period, the highest proportion of time was characterized by the TPD (47.5%), mainly in the CAP, Mendeleev Ridge, and Canada Basin east of the ridge, when ice density was high. The average northward velocity was 5.1 cm/s between 79.41°N and 86.32°N. The drift velocity was 7.3 cm/s north of 85°N, and the drift direction was northeastward. The TPD varied significantly in different sea areas.

The average surface velocity of the CSC was 13.5 cm/s. While this current moved westward along the slope, it also extended west-northward across the continental slope and flowed into the deep sea. This proved that Pacific water enters the Chukchi Sea with the CSC and is further transported across the continental shelf, directly contributing to the melting of ice in the CAP.

Clockwise spirals or waves in buoy trajectories are caused by inertial flow and when ice concentration is <50%, the effect of this flow is more significant. The observed inertial flow reached a maximum of 26 cm/s, and the radius of the inertial circle was 3.6 km. The magnitude of the inertial flow is independent of the average residual current but is related to the ice-free conditions of the sea.

When the sea surface is open, the disorganized surface flow occurs for a relatively long time under the direct influence of changeable surface winds. This phenomenon accounted for 32.8% of the whole observation period. The average velocity of the disorganized flow was similar to that in other sections. This result showed that the geostrophic current is weak in the CAP and western Canada Basin east of the Mendeleev ridge, and that the wind has a significant effect on the current. Under the conditions of variable wind field, the surface current is complex and variable.

At the end of the ice period and ice melting period, a surface westward flow started from the Canada Basin, crossed the Mendeleev ridge, and reached the Makarov basin in the range of 79°–80°N, 175°E–168°W. This cross-ridge surface flow was influenced by the sea surface wind and sea ice concentration. Through it, Pacific water is transported from the Canada Basin to the Makarov Basin.

The above findings are the main results of surface current observations conducted in the Arctic Ocean using a surface drifting buoy (No. 3002340107001500). The data obtained demonstrate that this buoy performed well in high latitude, Arctic waters.

Considering that drifting buoys are rarely used to observe currents in the Arctic Ocean, this experimental application demonstrates that these instruments can fully adapt to the conversion between sea ice. As they are equipped with a variety of observation tools, drifting buoys can carry out long-term and large-scale Lagrangian observations of surface currents and environmental elements of the upper ocean in polar seas.

References

Brugler E T, Pickart R S, Moore G W K, et al. 2014. Seasonal to interannual variability of the Pacific water boundary current in the Beaufort Sea. Progress in Oceanography, 127: 1–20, doi: 10.1016/j.pocean.2014.05.002

Centurioni L R. 2018. Drifter technology and impacts for sea surface temperature, sea-level pressure, and ocean circulation studies. In: Venkatesan R, Tandon A, D'Asaro E, et al, eds. Observing the Oceans in Real Time. Cham: Springer, 37–57,doi: 10.1007/978-3-319-66493-4_3

Centurioni L, Braasch L, Di Lauro E, et al. 2017. A new strategic wave

measurement station off Naples port main breakwater. Coastal Engineering Proceedings, 1(35): waves. 36, doi: 10.9753/icce.v35.waves.36
Chen Hongxia, Yang Wangxiao, Lin Lina, et al. 2021. Design and experimental application of surface drift buoy based on GNSS and Iridium communication. Journal of Ocean Technology (in Chinese), 40(4): 8–15, doi: 10.3969/j.issn.1003-2029.2021.04.002
Corlett W B, Pickart R S. 2017. The Chukchi slope current. Progress in Oceanography, 153: 50–65, doi: 10.1016/j.pocean.2017.04.005
Gong D L, Pickart R S. 2015. Summertime circulation in the eastern Chukchi Sea. Deep-Sea Research Part II: Topical Studies in Oceanography, 118: 18–31, doi: 10.1016/j.dsr2.2015.02.006
Haller M, Brümmer B, Müller G. 2014. Atmosphere–ice forcing in the transpolar drift stream: results from the DAMOCLES ice-buoy campaigns 2007–2009. The Cryosphere, 8(1): 275–288, doi: 10.5194/tc-8-275-2014
He Yan, Liu Na, Chen Hongxia, et al. 2015. Observed features of temperature, salinity and current in central Chukchi Sea during the summer of 2012. Acta Oceanologica Sinica, 34(5): 51–59, doi: 10.1007/s13131-015-0642-7
Jones E P, Swift J H, Anderson L G, et al. 2003. Tracing Pacific water in the North Atlantic ocean. Journal of Geophysical Research: Atmospheres, 108(C4): 3116, doi: 10.1029/2001JC001141
Kikuchi T, Itoh M, Nishino S, et al. 2015. Mooring-based long-term observation of oceanographic condition in the Chukchi Sea and Canada Basin of the Arctic Ocean. In: EGU General Assembly 2015. Vienna, Austria: EGU
Killworth P D, Smith J M. 1984. A one-and-a-half dimensional model for the Arctic halocline. Deep-Sea Research Part A. Oceanographic Research Papers, 31(3): 271–293, doi: 10.1016/0198-0149(84)90105-5
Lei Ruibo, Hoppmann M, Cheng Bin, et al. 2021. Seasonal changes in sea ice kinematics and deformation in the Pacific sector of the Arctic Ocean in 2018/19. The Cryosphere, 15(3): 1321–1341, doi: 10.5194/tc-15-1321-2021
Li Min, Pickart R S, Spall M A, et al. 2019. Circulation of the Chukchi Sea shelfbreak and slope from moored timeseries. Progress in Oceanography, 172: 14–33, doi: 10.1016/j.pocean.2019.01.002
Liu Haifeng. 2014. Analysis of Fram Strait inertial flow characters and physical mechanism of its generation and change (in Chinese)[dissertation]. Qingdao: Ocean University of China
Pickart R S, Moore G W K, Mao Chongyuan, et al. 2016. Circulation of winter water on the Chukchi shelf in early Summer. Deep-Sea Research Part II: Topical Studies in Oceanography, 130: 56–75, doi: 10.1016/j.dsr2.2016.05.001
Poulain P M, Luther D S, Patzert W C. 1992. Deriving inertial wave characteristics from surface drifter velocities: Frequency variability in the tropical Pacific. Journal of Geophysical Research: Oceans, 97(C11): 17947–17959, doi: 10.1029/92JC01381
Shi Jiuxin, Zhao Jinping, Jiao Yutian, et al. 2004. Pacific inflow and its links with abnormal variations in the Arctic Ocean. Chinese Journal of Polar Research (in Chinese), 16(3): 253–260
Shu Qi, Ma Hongyu, Qiao Fanli. 2012. Observation and simulation of a floe drift near the North Pole. Ocean Dynamics, 62(8): 1195–1200, doi: 10.1007/s10236-012-0554-4
Steele M, Zhang Jinlun, Ermold W. 2010. Mechanisms of summertime upper Arctic ocean warming and the effect on sea ice melt. Journal of Geophysical Research: Oceans, 115(C11): C11004, doi: 10.1029/2009JC005849
Sverdrup H U, Johnson M W, Fleming R H. 1942. The Oceans Their Physics, Chemistry, and General Biology. New York: Prentice-Hall
Thomson R E, LeBlond P H, Rabinovich A B. 1998. Satellite-tracked drifter measurement of inertial and semidiurnal currents in the northeast Pacific. Journal of Geophysical Research: Oceans, 103(C1): 1039–1052, doi: 10.1029/97JC02374
Tian Yin, Bai Xuezhi, Huang Yingqi. 2021. Analysis of the variation in intensity and source region of the Arctic Transpolar Drift. Chinese Journal of Polar Research (in Chinese), 33(4): 529–544, doi: 10.13679/j.jdyj.20210034
Tomczak M, Godfrey J S. 1994. Regional Oceanography: An Introduction. Oxford: Pergamon, doi: 10.1016/C2009-0-14825-0
Wang Huiwu, Chen Hongxia, Lv Liangang, et al. 2011. Study of tide and residual current observations in Chukchi Sea in the summer 2008. Acta Oceanologica Sinica (in Chinese), 33(6): 1–8
Wang Huiwu, Liu Na, Zhao Chang, et al. 2012. Distribution characteristics of residual current in the Chukchi Sea in Summer 2008. Advances in Marine Science (in Chinese), 30(3): 338–346
Webster F. 1968. Observations of inertial-period motions in the deep sea. Reviews of Geophysics, 6(4): 473–490, doi: 10.1029/rg006i004p00473
Weingartner T, Aagaard K, Woodgate R, et al. 2005. Circulation on the north central Chukchi Sea shelf. Deep-Sea Research Part II: Topical Studies in Oceanography, 52(24–26): 3150–3174, doi: 10.1016/j.dsr2.2005.10.015
Woodgate R A, Aagaard K, Swift J H, et al. 2007. Atlantic water circulation over the Mendeleev Ridge and Chukchi Borderland from thermohaline intrusions and water mass properties. Journal of Geophysical Research: Oceans, 112(C2): C02005, doi: 10.1029/2005JC003416
Woodgate R A, Weingartner T J, Lindsay R. 2012. Observed increases in Bering Strait oceanic fluxes from the Pacific to the Arctic from 2001 to 2011 and their impacts on the Arctic ocean water column. Geophysical Research Letters, 39(24): L24603, doi: 10.1029/2012gl054092
Yi Feng, Liu Bin, Li Zhonghan, et al. 2019. The impact of ocean turbulence on acquisition and processing of seismic data. Chinese Journal of Engineering Geophysics (in Chinese), 16(6): 775–783
Zhao Song, Dong Linsen, Wang Xiangqin, et al. 2020. Composition and provenance analysis of rare-earth elements in the manganese-rich brown layers of the Mendeleev Ridge, Arctic Ocean. Haiyang Xuebao (in Chinese), 42(7): 78–92
Zhao Yunxia, Wei Zexun, Wang Xinyi. 2011. Study of inertial motions using surface trajectories of Argo floats. Journal of Ocean Technology (in Chinese), 30(2): 72–75

Supplementary information:

Fig. S1. Map of the Arctic Ocean and surrounding seas. Orange arrows highlight the location of two surface currents, whose names are labeled white and abbreviated as follows: BG, Beaufort Gyre; TPD, Transpolar Drift. Many places are labeled with abbreviations: BS, Bering Strait; BC, Barrow Canyon; CAP, Chukchi Abyssal Plain; MR, Mendeleev Ridge; MB, Makarov Basin; NR, Northwind Ridge; CP, Chukchi Plateau.

Fig. S2. Monthly mean sea ice concentration from September to December 2019 and from July to October 2020. The drifter trajectories of the buoy are superimposed on the figure in yellow.

The supplementary information is available online at https://doi.org/10.1007/s13131-023-2202-x and http://www.aosocean.com/. The supplementary information is published as submitted, without typesetting or editing. The responsibility for scientific accuracy and content remains entirely with the authors.